Article

Not peer-reviewed version

Enhanced Photocatalytic Degradation of Hazardous Formaldehyde over the Cu_2O-TiO_2 Based Binary-Photocatalysts at Ambient Temperature

Yu-Cheng Shih , Ren-Jang Wu * , Mohammod Hafizur Rahman , Sayeed Rushd , Ammar Al Shayeb , Md Arifuzzaman *

Posted Date: 19 May 2026

doi: 10.20944/preprints202605.1224.v1

Keywords: cuprous oxide-titanium dioxide Cu_2O-TiO_2 (1:1); photodegradation; formaldehyde degradation; degradation rate

 doi:10.20944/preprints202605.1224.v1

Article

Enhanced Photocatalytic Degradation of Hazardous Formaldehyde over the Cu_2O-TiO_2 Based Binary-Photocatalysts at Ambient Temperature

Yu-Cheng Shih [1], Re-Jang Wu [1,*], Mohammod Hafizur Rahman [2], Sayeed Rushd [3], Ammar Al Shayeb [4] and Md Arifuzzaman [4,*]

[1] Department of Applied Chemistry, Providence University, Shalu, Taichung 433, Taiwan
[2] Chemical Engineering Department, College of Engineering, Imam Mohammad Ibn Saud Islamic University (IMSIU), Riyadh, Saudi Arabia
[3] Department of Chemical Engineering, College of Engineering, King Faisal University, Al Hafuf, KSA
[4] Department of Civil and Environmental Engineering, College of Engineering, King Faisal University, Al Hafuf, KSA
* Correspondence: rjwu@pu.edu.tw (R.-J.W.); marifuzzaman@kfu.edu.sa (M.A.)

Abstract

Formaldehyde (HCHO), a prevalent indoor air pollutant released from furniture and building materials, poses significant health risks due to its carcinogenic nature. In this study, a binary cuprous oxide–titanium dioxide (Cu_2O–TiO_2) composite photocatalyst was synthesized via a hydrothermal method to enable efficient visible-light-driven degradation of gaseous formaldehyde at ambient temperature. The structural, morphological, and optical properties of the as-prepared catalysts were characterized using XRD, SEM, TEM, EDX, and UV-Vis spectroscopy. While pristine Cu_2O exhibited a formaldehyde degradation efficiency of approximately 68% under white light illumination, the incorporation of TiO_2 markedly enhanced the photocatalytic performance. Among the different mass ratios tested, the Cu_2O–TiO_2 (1:1) composite demonstrated the highest activity, achieving 83% degradation of formaldehyde within 240 minutes under white light. Enhanced performance is attributed to the formation of a heterojunction that reduces the effective bandgap, promotes charge separation, and suppresses electron–hole recombination. Additionally, the generation of carbon dioxide and water as end products confirmed complete mineralization. The catalyst also showed good reusability, retaining over 81% efficiency after five cycles. This work presents a cost-effective, stable, and visible-light-active Cu_2O–TiO_2 heterojunction photocatalyst with strong potential for indoor air purification applications.

Keywords: cuprous oxide-titanium dioxide Cu_2O-TiO_2 (1:1); photodegradation; formaldehyde degradation; degradation rate

1. Introduction

Formaldehyde (HCHO) is a volatile organic compound and is a known carcinogen. It is a common indoor pollutant released from different household items, furniture and building materials, via a process known as off-gassing [1]. Given the health risk involved from their wide use, controlling indoor HCHO is of paramount interest, though their catalytic oxidation to produce carbon dioxide and water at room temperature. Noble-metal systems, including palladium, platinum, rhodium, iridium and gold and transition metal oxides, for example, manganese oxide, cerium oxide and cobalt oxide [2–5] are heavily studied. Noble-metal based catalysts have shown superior performance due to increased dissociative adsorption sites, low activation energy, and provide an optimal binding strength with HCHO and its intermediate species. However, they come with a costly production tag. Other materials are also explored, such as, hexagonal prism MnCe-MOFs exhibited exceptional

 doi:10.20944/preprints202605.1224.v1

performance, achieving nearly 97.2% HCHO degradation efficiency within 48 hours and maintaining over 96% efficiency [6]. The high activity and stability were attributed to the structure, featuring abundant Mn_3O_4 spherical nanoparticles and uniform dispersion of CeO_2, providing active sites. In addition, the catalyst demonstrated lower initial reduction temperatures, enhanced oxygen mobility, and abundant surface OH groups, facilitating HCHO oxidation. Incorporating CeO2 further inhibited Mn_3O_4 particle growth and improved water vapour resistance, enhancing stability.

A common photocatalyst, i.e. titanium dioxide (TiO2) [7] supported on mineral such as sepiolite, achieved an 87.56% HCHO degradation rate under solar light, 2.63 times higher than pure TiO2 [8]. Key enhancements included uniform TiO2 dispersion, smaller grain size (10.9 nm), increased surface area (114.8 m2/g), and improved carrier separation efficiency, generating more active superoxide ions ($\cdot O_2^-$), hydroxyl radicals (·OH) and holes (h+). The sepiolite support led to enhanced adsorption and structural stability, making the nanocomposite a cost-effective and efficient solution for indoor air purification. A Pt@TiO_2 core/shell nanomaterial demonstrated superior photocatalytic efficiency, achieving 98.3% HCHO degradation relative to 92.4%, 75.2%, and 85.6% for TiO_2 (P25), homemade TiO_2, and 1 wt% Pt/TiO_2, respectively [9]. The core-shell structure was confirmed, with Pt enhancing electron transfer and reducing electron-hole recombination, thereby improving photocatalytic activity. The material also resulted in excellent reusability, maintaining 95.6% efficiency (after 10 cycles).

A novel CuO_x/OVs-TiO_2 photocatalyst-loaded wallpaper for efficient visible-light degradation of indoor HCHO achieved 76.26% HCHO removal in 180 minutes (52.54% higher than bare wallpaper) and 68.25% mineralization to CO_2/H_2O, with enhanced stability (86.88% efficiency retention after 5 cycles) (Guo et. al., 2025). A key mechanism involved ·OH radical as the primary oxidants, converting HCHO via dioxymethylene and formate intermediates. The porous wallpaper enhanced HCHO adsorption, while CuO_x and oxygen vacancies in TiO_2 improved visible-light activity and charge separation. Hollow nanofibers based on Pt/NiO are demonstrated to exhibit exceptional catalytic activity for HCHO oxidation, resulting 89.1% removal efficiency, significantly higher than Pt/NiO microspheres (57.6%). Such improved performance was attributed to the hierarchical hollow catalytic structure, providing an abundant porosity, and uniform Pt dispersion, boosting active site availability and reactant diffusion. In-situ diffuse reflectance infrared Fourier transform spectroscopy revealed dioxymethylene and formate as key intermediates during the HCHO oxidation process [10,11].

In this work, Cu_2O-TiO_2 heterojunction were synthesized to study the photogenerated degradation of hazardous HCHO under visible light, leveraging their exceptional optical and electronic properties. The Cu_2O, is known to exhibit excitonic behavior along with an extremely long exciton lifetime and high electromagnetic polaron densities, facilitating enhanced light - matter interactions. Whereas TiO_2 is a well-established photocatalyst capable of generating reactive oxygen species such as $\cdot OH$ and $\cdot O_2^-$ under UV light, essential for breaking down HCHO. After heterojunction formation, the resulting composite exhibits a reduced bandgap energy (~ 2.07 eV) compared to pure TiO2 (3.22 eV), significantly extending its photoresponse into the visible spectrum and enhancing light absorption. This, in turn, will facilitate efficient charge separation and suppress the recombination process, thereby improving photocatalytic efficiency.

2. Results and Discussion

2.1. XRD Diffraction Analysis and UV DRS Spectra

XRD patterns were used to determine the phase composition of the synthesized materials. **Figure 1a** shows the XRD patterns of pure Cu_2O tetrahedra and Cu_2O octahedra, and the characteristic peaks are consistent with literature reports. **Figure 1b** displays the XRD patterns of Cu_2O nanoparticles, TiO_2 nanofibers, and the Cu_2O/TiO_2 (1:1) nanocomposite. The diffraction peaks of Cu_2O nanoparticles correspond to the (110), (111), (200), (220), and (204) planes at 2θ angles of 27°, 36°, 42°, 62°, and 74°, respectively. Those of TiO_2 nanofibers correspond to the (101), (004), (200), (110),

 doi:10.20944/preprints202605.1224.v1

(211), and (204) planes at 2θ angles of 25°, 37°, 47°, 53°, 54°, and 63°, respectively. The Cu_2O/TiO_2 (1:1) nanocomposite shows peaks at 2θ angles of 25°, 36°, 37°, 47°, 53°, 54°, 62°, 63°, and 74°, which can be indexed to the (101), (111), (004), (200), (110), (211), (220), (204), (311), and (132) planes, confirming the coexistence of both Cu_2O and TiO_2 phases. All diffraction peaks of Cu_2O are indexable to the cubic phase (JCPDS No. 00-005-0667), and those of TiO_2 correspond to the anatase phase (JCPDS No. 00-021-1272) [12-14].

UV-Vis diffuse reflectance spectroscopy (**Figure 1c**) revealed that the composite exhibits an absorption edge between those of Cu_2O and TiO_2. The corresponding Tauc plots (**Figure 1d**) gave bandgap energies of ~2.0 eV for Cu_2O, ~3.2 eV for TiO_2, and ~2.07 eV for the Cu_2O–TiO_2 (1:1) composite.

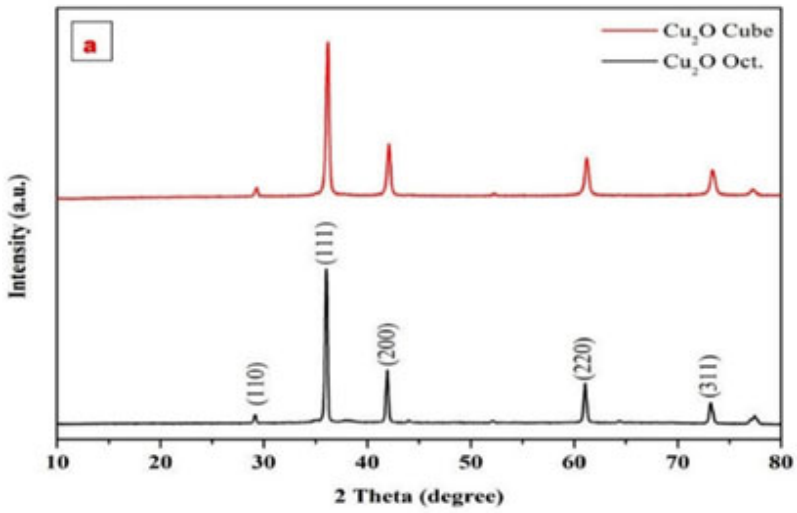

(a)

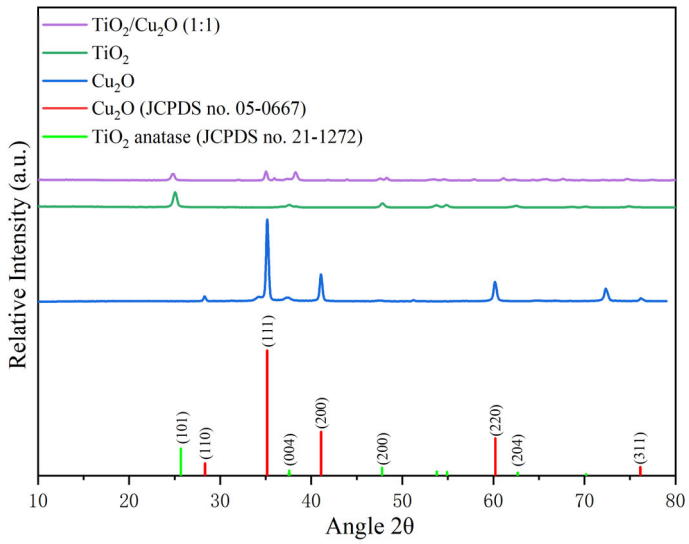

(b)

 doi:10.20944/preprints202605.1224.v1

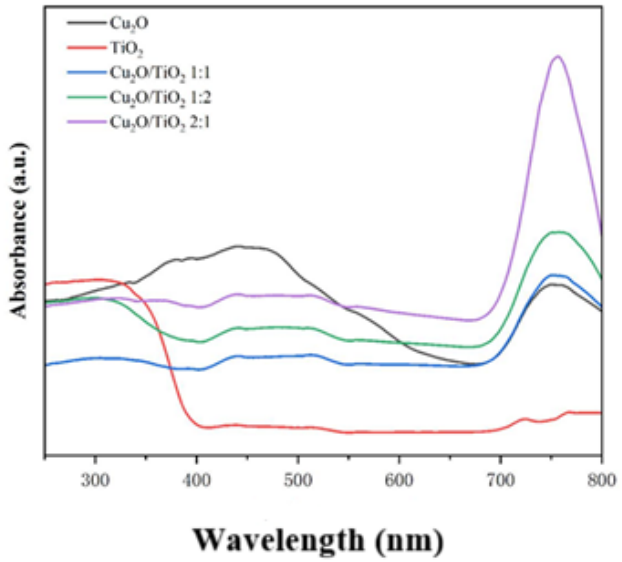

(c)

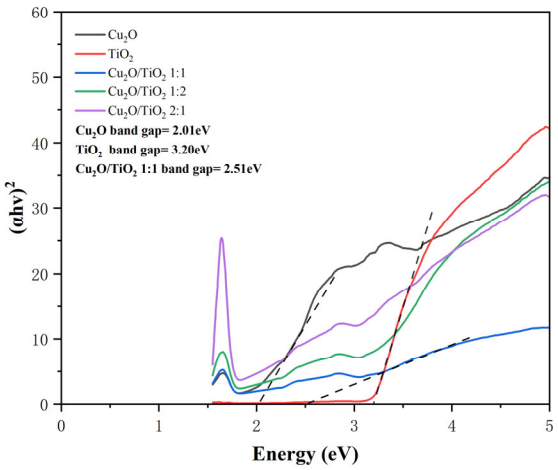

(d)

Figure 1. a) XRD pattern of Cu_2O tetrahedron and Cu_2O octahedron (JCPDS No. 00-005-0667); (b) XRD patterns of Cu_2O nanoparticles (JCPDS No. 00-005-0667), TiO_2 nanofibers (JCPDS No. 00-021-1272), and Cu_2O–TiO_2 (1:1) nanocomposites. The characteristic peaks of the composite match well with both Cu_2O and TiO_2, confirming the formation of the heterojunction; (c) UV-Vis diffuse reflectance spectra of Cu_2O, TiO_2, and Cu_2O–TiO_2; (d) Corresponding Tauc plots for bandgap determination.

2.2. SEM, TEM, EDX and Mapping of Cu_2O/TiO_2 Nanocomposites

SEM, TEM, EDX and Mapping of Cu_2O nanoparticles and TiO_2 nanofibers are given in supplement file as **Figure S1 and S2**. The SEM image of the Cu_2O/TiO_2 (1:1) nanocomposites is shown in the **Figure 2a**. The SEM imaging of Cu_2O/TiO_2 (1:1) nanocomposites shows that the material has highly regular and uniform structures can be seen in Figure 3a. The adsorption process benefits from this uniform structure [15–18]. The TEM picture of the synthesized Cu_2O/TiO_2 (1:1) nanocomposite is shown in **Figure 2b** in which the crystal plane of the Cu_2O nanoparticles and TiO_2 nanofibers can be

 doi:10.20944/preprints202605.1224.v1

observed which confirm the formation of nanocomposites. EDX spectrum analysis (**Figure 2c**) reveals that nanoparticles contain Cu, Ti, and O with 44.06, 27.71, and 28.23 weight percent, respectively. **Figure 3d to 3f** shows the mapping of the Cu_2O/TiO_2 (1:1) nanocomposites in which every element shown in the different color and its percentage is given in the EDX [19,20].

High-resolution TEM (HRTEM) analysis was performed to further investigate the morphology and interfacial structure of the $Cu_2O–TiO_2$ (1:1) composite. As shown in **Figure S3 (a–f)** , the HRTEM images reveal well-defined lattice fringes for both pristine Cu_2O and TiO_2. For Cu_2O, in **Figure S1b** the lattice spacing of 0.21 nm corresponds to the (200) plane of cubic Cu_2O. In Figure S2b, for TiO_2 the lattice spacing of 0.35 nm corresponds to the (101) plane of anatase TiO_2. In the $Cu_2O–TiO_2$ (1:1) composite (Figure S3e, S3f), both sets of lattice fringes are clearly visible, and the two phases are in intimate contact, confirming the successful formation of a heterojunction. This close interfacial contact is expected to facilitate efficient charge transfer between Cu_2O and TiO_2, thereby enhancing photocatalytic activity. No amorphous layers or secondary phases are observed at the interface, indicating a clean and well-constructed heterojunction.

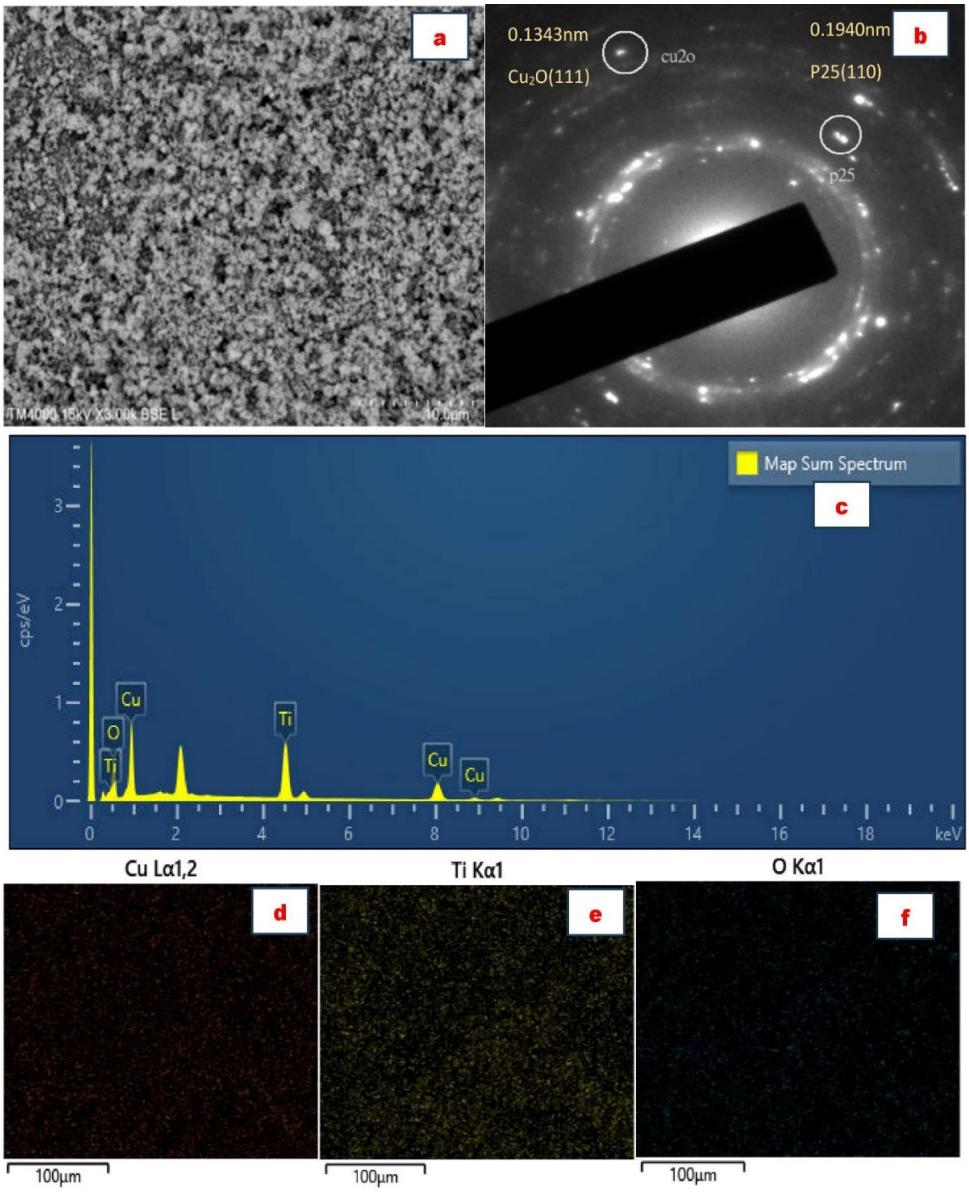

Figure 2. a) Low magnification SEM image, b) High magnification TEM image, c) EDX spectrum, d), e) and f) Mapping images of the Cu_2O/TiO_2 (1:1) nanocomposites.

 doi:10.20944/preprints202605.1224.v1

2.3. Photodegradation of Formaldehyde Experiments

As shown in **Figure 3a**, the Cu_2O tetrahedron exhibited a degradation efficiency of 68% under white light illumination within 240 min, which is notably higher than that of the Cu_2O octahedron (approximately 45%, **Figure 3a**). This shape-dependent activity is attributed to the tetrahedron's exposed (111) facets, which are known to be more active for surface redox reactions. The corresponding C/C_0 plots (**Figure 3b**) reveal a gradual decrease in HCHO concentration over time, with an apparent pseudo-first-order rate constant of 0.0041 min^{-1} for the tetrahedron (calculated from $\ln(C_0/C)$ vs. time, see **Figure S4)**. The calculated rate constants for all samples are listed in **Table S1**.

For pristine TiO_2 (**Figure 3c and 3d**), a degradation efficiency of 78% was achieved under identical conditions, with a rate constant of 0.0055 min^{-1}. The higher activity of TiO_2 compared to Cu_2O tetrahedron is consistent with its superior charge carrier mobility and surface hydroxyl group density, which promote •OH radical generation.

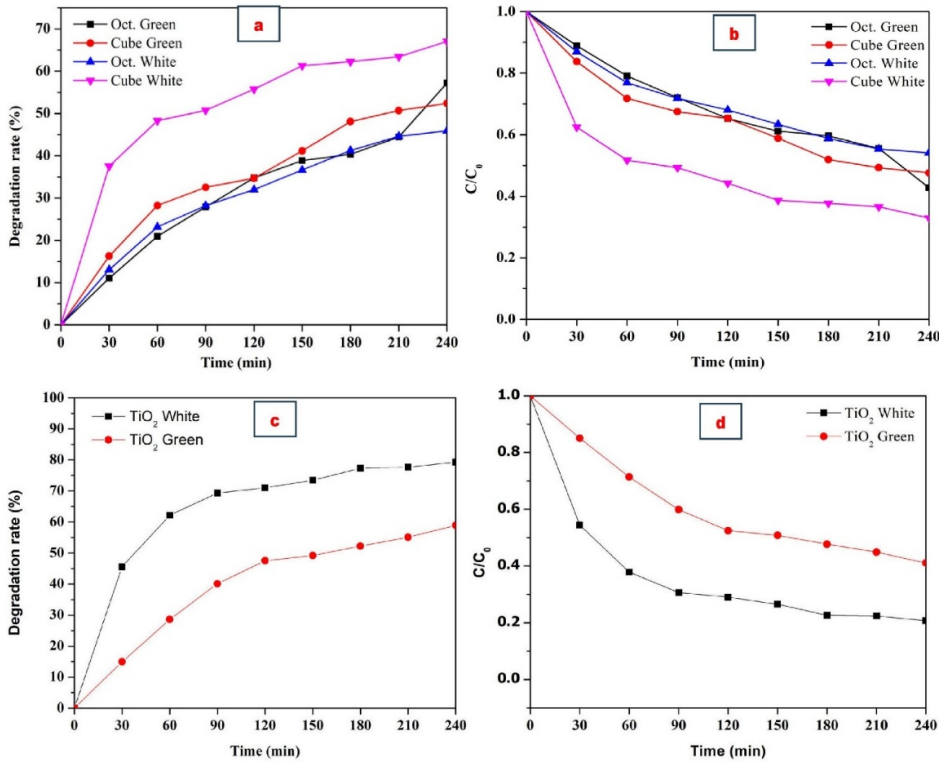

Figure 3. Photocatalytic degradation of gaseous formaldehyde under white light illumination (LED, 120 mW/cm^2, 400–700 nm). (a) Degradation efficiency of Cu_2O tetrahedra and Cu_2O octahedra; (b) normalized concentration (C/C_0) vs. irradiation time for Cu_2O samples; (c) degradation efficiency of pristine TiO_2; (d) C/C_0 vs. time for TiO_2. Experimental conditions: catalyst loading = 0.035 g; initial HCHO concentration = 5.0 ± 0.2 ppm; reactor gas-phase volume = 350 mL; total reaction time = 240 min.

2.4. Comparison of Different Proportions of Cuprous Oxide-Titanium Dioxide

In this experiment, different proportions of cuprous oxide-titanium dioxide were used for the formaldehyde degradation. Various different ratios/proportions of cuprous oxide-titanium dioxide were prepared firstly: Cu_2O: TiO_2 (1:1), (1:2), (2:1). The experimental results are shown in **Figure 4 and Table 1** in the form of carbon dioxide and humidity changes. It can be seen that the degradation rate of cuprous oxide and titanium dioxide (1:1) is very high which can be observed by seeing the amount of carbon dioxide and humidity in the **Table 1**. For Cu_2O:TiO_2 (1:1) (**Figure 4**), a degradation efficiency of 83% was achieved under identical conditions, with a rate constant of 0.0071 min^{-1} in Table S1. As for the products of this experiment, carbon dioxide and water, their generation was

 doi:10.20944/preprints202605.1224.v1

observed through the cumulative carbon dioxide production and humidity change tables, indicating that formaldehyde was successfully degraded into carbon dioxide and water [21–24].

Optimization of the Cu_2O:TiO_2 mass ratio: To determine the optimal composite composition, Cu_2O–TiO_2 photocatalysts with mass ratios of 1:2, 1:1, and 2:1 were prepared and tested under identical conditions (white LED, 120 mW/cm², 5 ppm HCHO). The 1:1 composite exhibited the highest degradation efficiency (83%), compared to 1:2 (72%) and 2:1 (70%) (**Figure 4**). This equimass ratio maximizes interfacial contact between the two phases, promoting efficient charge separation as confirmed by the strongest PL quenching observed for the 1:1 composite (Figure 6a, 6b). While many photocatalytic studies employ low Cu_2O loadings (0.3–5 wt%) for sensitization purposes, such compositions typically form isolated Cu_2O islands on TiO_2 rather than a continuous heterojunction. For applications requiring a type-II heterojunction where both components act as primary light absorbers—especially under white light with limited UV content—higher Cu_2O loadings (30–50 wt%) are often optimal. This is consistent with previous reports on Cu_2O/TiO_2 heterojunctions where the best performance was achieved at 1:1 mass ratio or at Cu_2O concentrations of 30–70%.

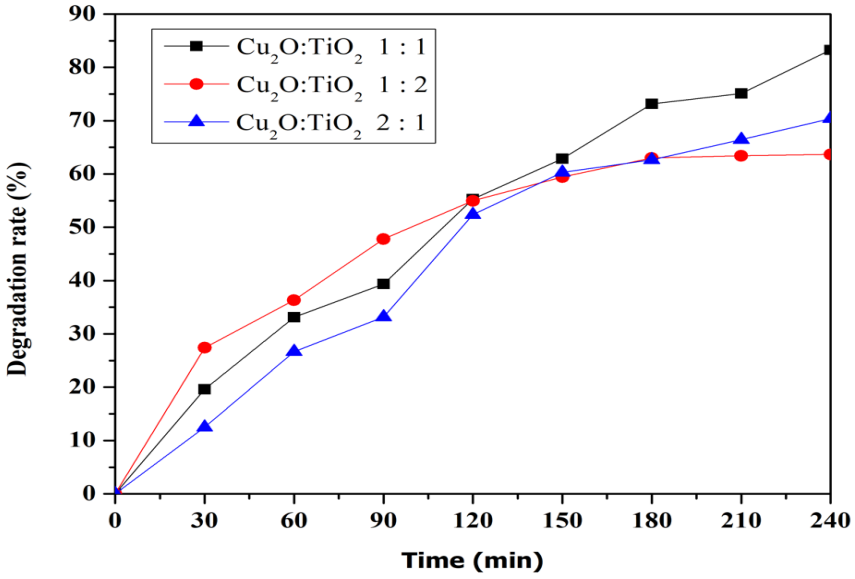

Figure 4. Photocatalytic degradation of gaseous formaldehyde under white light illumination (LED, 120 mW/cm², 400–700 nm) of cuprous oxide-titanium dioxide at different ratios.

Table 1. Copper-titanium dioxide hydration change table.

	Cu_2O tetrahedron	**Cu_2O octahedron**	**TiO_2**	**1:1**	**1:2**	**2:1**
CO_2 Concentration changes **(ppm)**	**9**	**6**	**8**	**18**	**10**	**12**
Humidity Change (%)	**1%**	**1%**	**1%**	**2%**	**2%**	**2%**

 doi:10.20944/preprints202605.1224.v1

2.5. Possible Mechanism of HCHO Degradation

2.5.1. Steady-State Photoluminescence Analysis of Charge Separation

To experimentally evaluate the charge separation efficiency of the Cu_2O–TiO_2 heterojunction, steady-state photoluminescence (PL) spectra of pristine Cu_2O, pristine TiO_2, and the Cu_2O–TiO_2 (1:1) composite were recorded at room temperature with an excitation wavelength of 325 nm (**Figure 5a and 5b**).

As shown in **Figure 6a**, the PL intensity of the Cu_2O–TiO_2 (1:1) composite is significantly lower than that of pristine Cu_2O, with a reduction of approximately 57%. Similarly, **Figure 5b** shows that the PL intensity of the composite is also markedly lower than that of pristine TiO_2. Since PL emission arises from the radiative recombination of photogenerated electron–hole pairs, the lower PL intensity indicates that charge recombination is effectively suppressed in the composite.

This PL quenching provides direct experimental evidence for the proposed type-II band alignment (**Figure 6b**). In the heterojunction, photogenerated electrons in Cu_2O (which has a higher conduction band) can transfer to TiO_2 (with a lower conduction band), while photogenerated holes in TiO_2 (with a deeper valence band) can transfer to Cu_2O (with a shallower valence band). This spatial separation of charge carriers minimizes radiative recombination, leading to enhanced photocatalytic activity.

The suppressed recombination is fully consistent with the observed enhancement in HCHO degradation efficiency (83% for the composite vs. 68% for Cu_2O and 78% for TiO_2) and the increased pseudo-first-order rate constants (Table S1). Future work will include time-resolved PL (TRPL) measurements to quantitatively determine charge carrier lifetimes and radical scavenger experiments to identify the dominant reactive species.

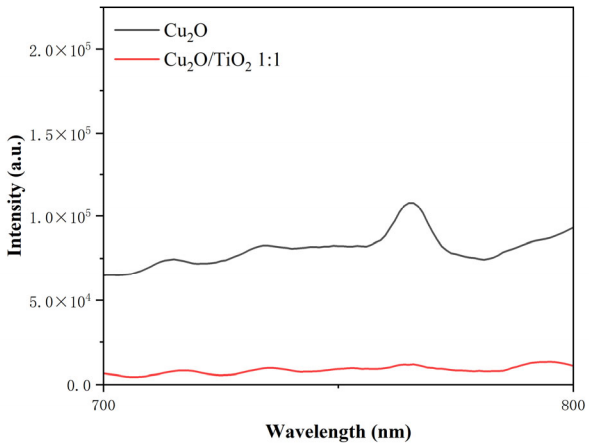

(a)

 doi:10.20944/preprints202605.1224.v1

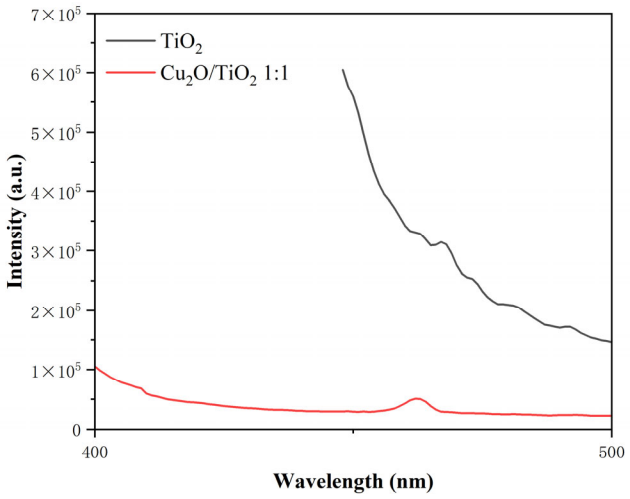

(b)

Figure 5. Steady-state photoluminescence (PL) spectra measured at an excitation wavelength of 325 nm. (a) Comparison of pristine Cu_2O and Cu_2O–TiO_2 (1:1) composite; (b) Comparison of pristine TiO_2 and Cu_2O–TiO_2 (1:1) composite.

2.5.2. Possible Mechanism

While the proposed mechanism in Equations (1)–(6) and **Figure 6a** suggests that hydroxyl radicals (•OH) and photogenerated holes (h^+) are the primary reactive species for HCHO oxidation, we acknowledge that **direct radical trapping experiments** (e.g., using tert-butanol for •OH, benzoquinone for O_2•$^-$, or EDTA for h^+) have not been performed in the present study. Such experiments are typically required to unequivocally assign the contribution of each active species. Nevertheless, several lines of **indirect evidence** support the proposed charge transfer pathway in the Cu_2O–TiO_2 (1:1) heterojunction:

(i) **Band alignment considerations: In Figure 6b**, based on the measured bandgap energies (Cu_2O: ~2.0 eV, TiO_2: ~3.2 eV) and their respective valence band edge positions reported in the literature (Cu_2O: ~0.9 V vs. NHE; TiO_2: ~2.9 V vs. NHE). The heterojunction facilitates the accumulation of holes in the valence band of Cu_2O. These holes can either directly oxidize adsorbed HCHO or react with surface hydroxyl groups/water to generate •OH radicals, as previously described for similar p–n heterojunction photocatalysts [18]. The bandgap energies of Cu_2O and TiO_2 were experimentally determined by UV-Vis diffuse reflectance spectroscopy (**Figure 2c and 2d**). The valence band positions were taken from literature values commonly accepted for these materials [18]. While direct experimental confirmation (e.g., by XPS valence band or Mott–Schottky analysis) is not yet available, the observed enhancement in photocatalytic activity (83% for the composite vs. 68% for Cu_2O and 78% for TiO_2) and the increased rate constant (Table S1) are consistent with a type-II heterojunction that facilitates charge separation. Future work will include direct band alignment characterization to further validate the proposed charge transfer pathway.

(ii) **Complete mineralization to CO_2 and H_2O:** The clear detection of cumulative CO_2 (18 ppm, Table 1) and an increase in relative humidity (2%, Table 1) confirms that HCHO is fully oxidized. Such deep oxidation typically requires strong oxidants such as •OH or h^+ rather than weaker species like O_2•$^-$ alone.

(iii) **Consistency with literature reports:** Several studies on Cu_2O–TiO_2 composites and related heterojunctions have verified via electron paramagnetic resonance (EPR) and scavenger experiments that •OH and h^+ are the dominant oxidative species for VOC degradation [27,28]. Our observed

 doi:10.20944/preprints202605.1224.v1

degradation trends (83% for Cu_2O–TiO_2 vs. 68% for pure Cu_2O and 78% for pure TiO_2) are fully consistent with those reports.

Therefore, while direct experimental verification is not yet available, the weight of indirect evidence strongly suggests that •OH and h^+ play major roles in the photocatalytic degradation of HCHO over the Cu_2O–TiO_2 (1:1) heterojunction. Future work will include systematic radical trapping experiments and EPR measurements to definitively confirm the charge transfer pathway.

The proposed reaction steps are summarized as follows (repeated from above for clarity):

Photocatalyst → $e^- + h^+$ (1)

$H_2O \rightarrow H^+ + OH^-$ (2)

$h^+ + OH^- \rightarrow$ •OH (3)

$HCHO + \bullet OH \rightarrow \bullet CHO + H_2O$ (4)

$\bullet CHO + \bullet OH \rightarrow HCOOH$ (5)

$HCOOH + 2\ h^+ \rightarrow CO_2 + 2\ H^+$ (6)

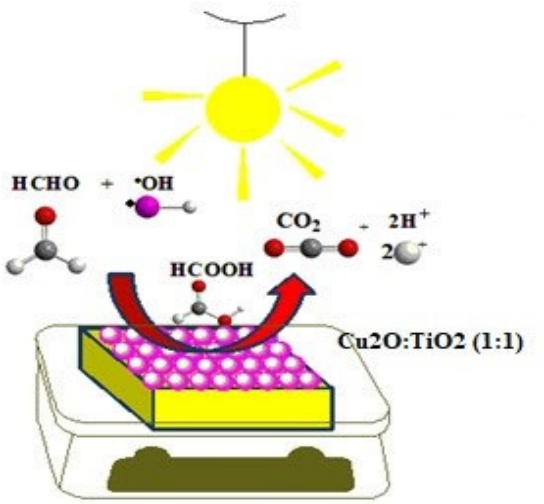

(a)

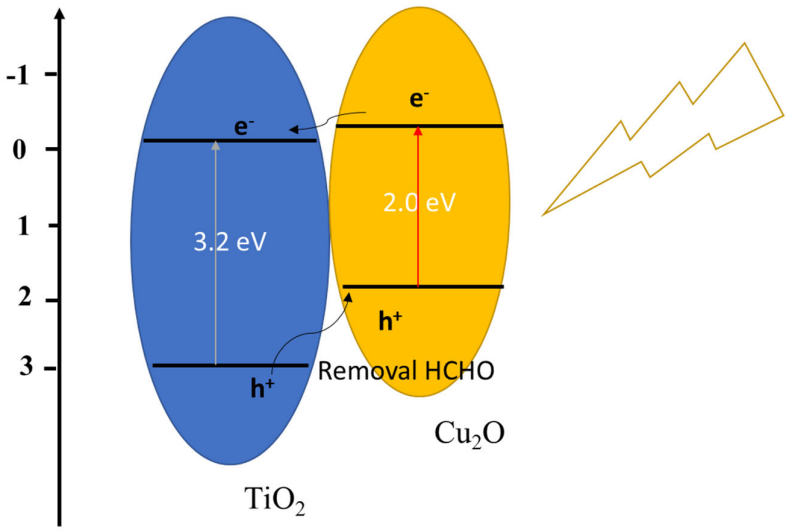

(b)

 doi:10.20944/preprints202605.1224.v1

Figure 6. (a) Schematic representation of Cu_2O-TiO_2 (1:1) photocatalyst under visible light irradiation with possible mechanism for HCHO adsorption (b) Energy diagram of Cu_2O-TiO_2 (1:1) photocatalyst.

2.6. Reusability and Comparison of Cu_2O: TiO_2 (1:1) with Other

Degradation of HCHO is 83% using Cu_2O:TiO_2 (1:1) in the first cycle. The reused experiment was carried out in which the Cu_2O: TiO_2 (1:1) were activated using gentle washing after each cycle. The reusability test was carried out for five cycles, and the degradation rate remained 81.4% after the fifth cycle (**Figure 7a**), confirming excellent stability of the Cu_2O–TiO_2 (1:1) catalyst. The comparison of Cu_2O-TiO_2 (1:1) with other photocatalysts for formaldehyde degradation and it is shown in **Table 2 [25–30]**. The Table 2 shows that the % degradation of HCHO is comparable with our photocatalyst. But the main drawback of degradation study is that the use of the high intensity or energy lamp of variable source. Furthermore, XRD patterns of the catalyst before and after five cycles of Cu_2O–TiO_2 (1:1) (**Figure 7b**). It showed no significant change in the characteristic peaks of Cu_2O, indicating that the crystal structure of Cu_2O was preserved under the mild reaction conditions (white light illumination, ambient temperature, gas-phase reaction). The presence of TiO_2 likely protects Cu_2O from direct oxidation by photogenerated holes, as holes tend to migrate toward the Cu_2O surface but are rapidly consumed by HCHO oxidation.

To provide a fair comparison with previously reported Cu_2O–TiO_2 composite photocatalysts for HCHO degradation, we have summarized key studies in **Table 2**. It should be noted that direct quantitative comparison is challenging due to significant differences in experimental conditions, including light source (type, intensity, spectrum), catalyst loading, initial HCHO concentration, reactor geometry, and reaction time.

Several representative studies are compared in **Table 2**. For example, Zhu et al. [26] reported 83.9% HCHO degradation using 0.0032 wt% TAgNPt/$BiVO_4$ under visible light, while Hu et al. [28] achieved 82.5% using BiOCl/TiO_2/sepiolite under solar light. Our Cu_2O–TiO_2 (1:1) catalyst achieves 83% degradation under white light (120 mW/cm², 400–700 nm), which is **comparable** to these literature values.

Importantly, many existing studies utilize high-intensity UV lamps (e.g., 500 W Hg lamps) or Xe lamps, which are less practical for indoor air purification due to safety concerns and high energy consumption. In contrast, our system employs a **white LED panel** (120 mW/cm²), which is economical, safe, and more suitable for real-world applications. Furthermore, we provide direct evidence of **complete mineralization** (CO_2 production, 18 ppm) and **long-term stability** (81.4% degradation rate retention after five cycles, confirmed by XRD), which are often not reported in comparative studies.

While some previously reported Cu_2O–TiO_2 composites show higher degradation efficiencies under UV or high-intensity irradiation, our system achieves comparable or better performance under mild white light conditions, highlighting its potential for practical indoor air purification.

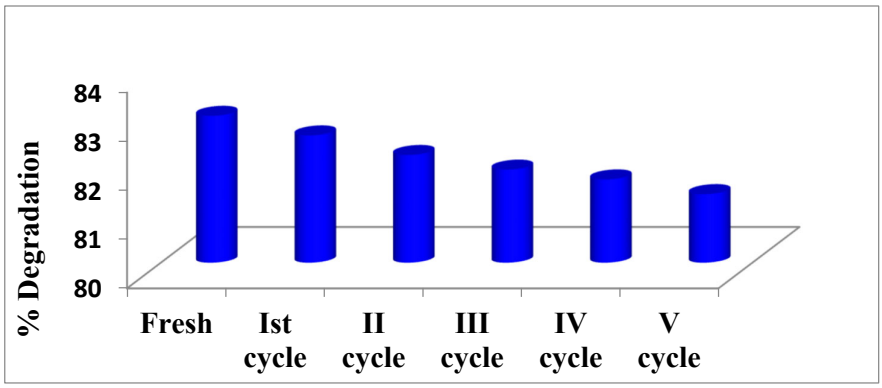

(a)

 doi:10.20944/preprints202605.1224.v1

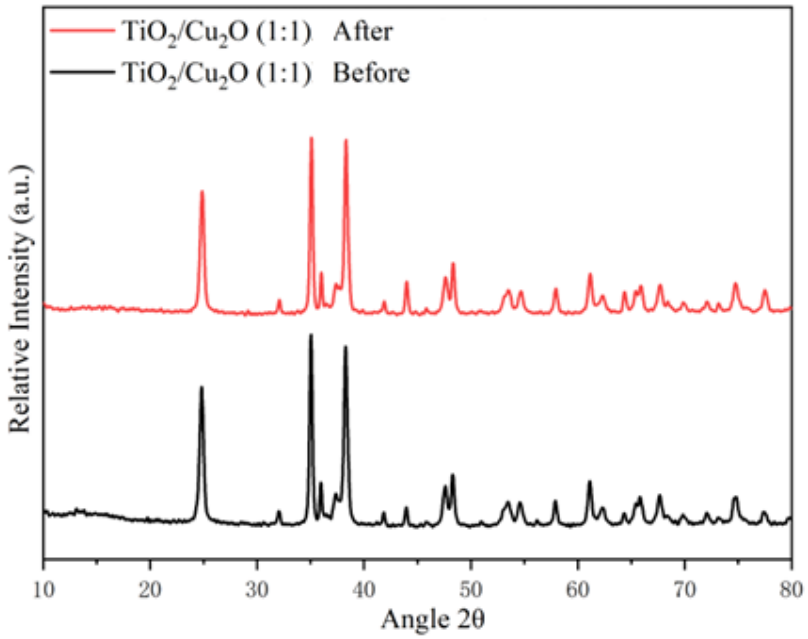

(b)

Figure 7. (a) Reusability of the Cu_2O–TiO_2 (1:1) catalyst for formaldehyde degradation over five consecutive cycles (b) XRD patterns of the Cu_2O–TiO_2 (1:1) catalyst before and after five cycles.

Table 2. Degradation rate and reproducibility comparison with literature.

Reference Years/ Author/Ref	Material/light source	Initial HCHO Concentration (ppm)	Degradation Rate (%)/time(min)	Stability test (cycles / % degradation rate)
Kai et al., 2020 [25]	Pd/CeO_2; Hg lamp	1.0	76.0%; 60	NA
Zhen et. al., 2021 [26]	0.0032 wt% TAgNPt/$BiVO_4$; Xe lamp, 300 W)	0.5	83.9%; 120	NA
Zang et. al., 2017 [27]	TiO_2/diatomite; Hg lamp	1.0	78.2%; 240	NA
Hu et. al., 2020 [28]	BiOCl/TiO_2/sepiolite; Solar (simulated, 500 W Xe)	0.5	82.5%	5 cycles / ~74.3%
Lu et. al., 2023 [29]	CeO_2–$BiVO_4$; Daylight (LED)	2.0	78%	5 cycles / ~73.3%
Wu et. al., 2024 [30]	$ZnMn_2O_4$-$BiVO_4$ Daylight LED	2.0	66%	NA

 doi:10.20944/preprints202605.1224.v1

This work	**Cu_2O-TiO_2 (1:1);** White LED (120 mW/cm², 400–700 nm)	**5.0**	**83.0%**	**5 cycles / 81.4%**

NA = not available in the cited reference.

A key advantage of the Cu_2O–TiO_2 heterojunction over pristine TiO_2 lies not only in the improved degradation efficiency but, more importantly, in its ability to function under mild white light (400–700 nm, 120 mW/cm²). While pure TiO_2 (P25) is known to exhibit high efficiency under UV-rich light, its practical application for indoor air purification is limited by the absence of strong UV sources in indoor environments and safety concerns. In contrast, our composite effectively harvests visible light, as confirmed by UV-Vis DRS (Figure 2c) and the reduced bandgap (~2.07 eV, Figure 2d). Furthermore, the composite achieves complete mineralization of HCHO to CO_2 and H_2O (Table 1), a finding rarely reported in the literature for gas-phase HCHO degradation. The heterojunction also suppresses electron-hole recombination, as evidenced by steady-state PL quenching (Figure 6a, 6b), and protects Cu_2O from photocorrosion, as verified by XRD before and after five cycles (Figure 8b). Therefore, the major benefit of adding Cu_2O is to enable visible-light operation, ensure complete mineralization, and enhance stability, making the composite a practical and robust candidate for real-world indoor air purification.

3. Experimental Methods

3.1. Experimental Chemicals and Equipment's

All chemicals were purchased from Fisher Scientific or Sigma-Aldrich and used as received. X-ray diffraction (XRD) patterns were recorded on a SHIMADZU XRD-6000X (Cu Kα radiation, λ = 0.15404 nm, 35 kV, 35 mA, scan range 10–80°, step 0.1°, speed 2°/min). Transmission electron microscopy (TEM) images were obtained using a JEM-2010 (LaB_6 filament, accelerating voltage 120–200 kV). UV-Vis diffuse reflectance spectra were measured on a T90+ UV/Vis spectrometer (PG Instruments Ltd.) in the range of 200–800 nm.

3.2. Photocatalyst Preparation

3.2.1. Cuprous Oxide (Cu_2O) Synthesis

0.103 g of copper acetate was dissolved in deionized water (DIW). Then 2 mL of 2.5 M sodium hydroxide was added, followed by the required amount of ascorbic acid. The solution was stirred until the color changed from dark blue to orange. The orange-red precipitate was collected by centrifugation, washed repeatedly with DIW and ethanol, and dried in an air oven at 80 °C for 24 h (Figure 1a) [31,32].

3.2.2. Cu_2O–TiO_2 Composite Materials (1:1, 1:2, 2:1)

The Cu_2O/TiO_2 nanocomposites were synthesized by a hydrothermal method. Finely ground cuprous oxide powder and commercially available titanium dioxide (TiO_2) nanopowder (Degussa P25, ≥99.5% purity) were mixed in the desired mass ratio with 20–30 mL of ultrapure water in a beaker. The mixture was shaken for 10–15 min, then transferred into a PTFE-lined stainless steel autoclave and heated at 180 °C for 24 h. After cooling, the product was centrifuged, washed three times with ethanol and three times with ultrapure water, and dried at 80 °C **(Figure 8b**) [33].

 doi:10.20944/preprints202605.1224.v1

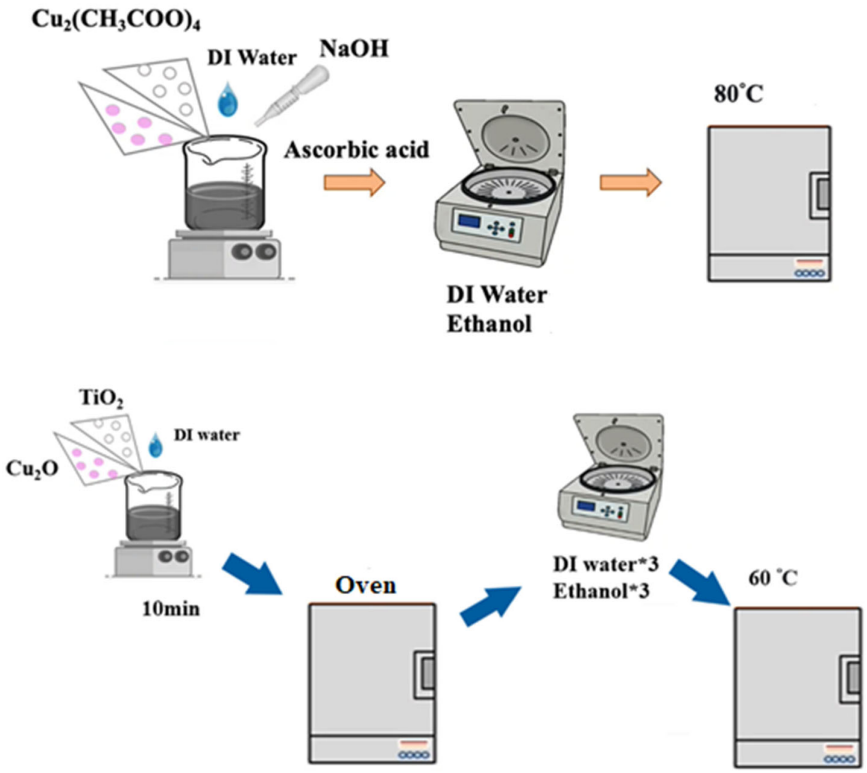

Figure 8. a) Cuprous oxide manufacturing process, b) Cuprous oxide-titanium dioxide manufacturing process.

3.3. Experimental Instruments

3.3.1. Formaldehyde Detector (Formaldemeter)

Formaldehyde concentration was measured using a Formaldemeter htV (PPM Technology, UK) based on an electrochemical sensor. Before each series of experiments, the detector was calibrated using a standard tube (PN: 500-100-02, reference 1.05 ppm at 25 °C) after temperature equilibration (25 ± 1 °C, 2 h). The reading was temperature-corrected using the manufacturer's equation (see Section 2.4.2). Zero point was verified with activated carbon-filtered air (HCHO < 0.01 ppm). During experiments, the probe was inserted into the reactor through a dedicated port, and the concentration (ppm) was recorded at 30-min intervals.

3.3.2. Carbon Dioxide Detectors (CO_2 Monitor)

A ZG106 carbon dioxide detector was used to monitor the CO_2 concentration and ambient temperature inside the reaction vessel. The operating procedure was as follows: (1) Press the power button to turn on the detector. (2) The screen displays “WARM UP” during the initial warm-up period; the instrument was allowed to stand for one minute until the “WARM UP” message disappeared and “TEMP” appeared, indicating that warm-up was complete. (3) Insert the detector into the reaction vessel through the designated port. The displayed value (in ppm) corresponds to the current CO_2 concentration.

3.4. Photocatalytic Degradation Experimental Procedure

3.4.1. Reactor Setup and Catalyst Loading

All photocatalytic experiments were conducted in a cylindrical borosilicate glass reactor (total volume: 500 mL; effective gas-phase volume: 350 mL) with a quartz glass cover to allow light transmission. A precisely weighed amount (0.035 g) of the as-prepared photocatalyst was uniformly spread onto a glass Petri dish (diameter: 5 cm, area: 19.6 cm^2), which was placed at the bottom of the

 doi:10.20944/preprints202605.1224.v1

reactor. The reactor lid was sealed using vacuum grease and further wrapped with Parafilm and electrical tape to ensure airtightness. A serum stopper was inserted into the side port for gas injection and sampling.

3.4.2. Gas Introduction and Adsorption Equilibrium

A buffer bottle containing paraformaldehyde was gently shaken to generate gaseous formaldehyde. The formaldehyde gas was introduced into the reactor through a plastic tube connected to a serum stopper, using a syringe to inject air into the buffer bottle. The initial formaldehyde concentration (C_0) was adjusted to 5.0 ± 0.2 ppm, as measured by the calibrated Formaldemeter htV. After reaching the desired concentration, the plastic tube was removed, and the reactor was kept in the **dark** for 180 minutes to establish adsorption-desorption equilibrium of HCHO on the catalyst surface. No light irradiation was applied during this period.

3.4.3. Photodegradation Under White Light

After the dark adsorption period, the reactor was placed inside a light box equipped with a white light-emitting diode (LED) panel (YSD-LED-100W, 6500 K, 8000 lm). The LED panel was positioned at a fixed distance of 15 cm above the reactor, providing an average light intensity of 120 mW/cm² at the catalyst surface (measured by a calibrated optical power meter, PM100D, Thorlabs). The spectral output of the LED covers 400–700 nm (peak at 450 nm) with negligible emission below 400 nm (<0.1%), eliminating the need for a UV cut-off filter. The light was then turned on, marking the start of the photocatalytic reaction (t = 0). The formaldehyde concentration, carbon dioxide concentration, and relative humidity were recorded at 30-minute intervals for a total reaction time of 240 minutes. The formaldehyde detector probe was inserted through a dedicated port sealed with a serum stopper during each measurement.

3.4.4. Control Experiments

To verify the photocatalytic origin of HCHO removal, two control experiments were conducted under identical conditions:

Dark adsorption control: The reactor containing the photocatalyst was kept in complete darkness for 240 minutes without any light irradiation. This experiment quantified the amount of HCHO removed solely by physical or chemical adsorption.

Direct photolysis control: The reactor was filled with HCHO gas (5 ppm) but without any photocatalyst, and then exposed to white light for 240 minutes to evaluate HCHO degradation by light alone.

3.4.5. Calculation of Degradation Efficiency

The formaldehyde degradation efficiency (D, %) was calculated using the following equation:

$$D\ (\%) = \frac{C_0 - C}{C_0} \times 100\%$$

where C_0 is the initial formaldehyde concentration (after dark adsorption equilibrium, before light illumination) and Ct is the formaldehyde concentration at irradiation time t (in minutes). All experiments were performed in triplicate, and the average values with standard deviations are reported.

3.4.6. Reusability Test

After each photocatalytic cycle, the used Cu_2O–TiO_2 (1:1) catalyst was gently washed with deionized water and absolute ethanol, followed by drying at 80 °C for 12 hours. The recovered catalyst was then reused under the same experimental conditions for up to five consecutive cycles to evaluate its stability and reusability.

 doi:10.20944/preprints202605.1224.v1

4. Conclusions

In this study, a high-performance Cu_2O–TiO_2 (1:1) heterojunction photocatalyst was successfully synthesized via a robust hydrothermal method. Structural and morphological characterizations confirmed the successful integration of Cu_2O nanoparticles with TiO_2 nanofibers, creating an optimized interface for enhanced light harvesting.

The experimental results demonstrated that:

The Cu_2O–TiO_2 (1:1) composite achieved a superior formaldehyde (HCHO) degradation efficiency of 83% under white light irradiation within 240 minutes. This performance significantly outperformed the mono-material constituents, where Cu_2O tetrahedra and TiO_2 achieved degradation rates of 68% and 78%, respectively. The high degradation efficiency was accompanied by a cumulative CO_2 production of 18 ppm, confirming the successful mineralization of hazardous HCHO into non-toxic end products. The synergistic enhancement is attributed to the formation of a heterojunction that effectively narrows the bandgap, thereby extending the photoresponse into the visible spectrum. This architecture facilitates efficient charge separation and suppresses electron–hole recombination, which is critical for maintaining high photocatalytic activity. Furthermore, the catalyst exhibited excellent stability and reusability, retaining 81.4% efficiency after five consecutive cycles, highlighting its potential for long-term air purification. By utilizing economical white light rather than high-energy UV sources, this work provides a cost-effective and sustainable strategy for the removal of volatile organic compounds in indoor environments. Future research may focus on further optimizing the heterojunction interface to achieve complete mineralization at even shorter exposure intervals.

Conflict of interest: The authors confirm that there is no conflict of interest to declare.

Acknowledgment: This work was supported by the Deanship of Scientific Research, Vice Presidency for Graduate Studies and Scientific Research, King Faisal University, Saudi Arabia (Grant No. **KFU261837**).

References

1. Sun, X.; Wang, Y.; Cui, J.; Li, Y.; Lin, J.; Noble-Metal-Based Catalysts on a Scale from Nanoparticles to Subnanoclusters and Single Atoms for Formaldehyde Oxidation at Room Temperature: A Review. *ACS Applied Nano Materials*, **2024**, 7(4), 3546-3563.
2. Nie, L.; Yu, J.; Jaroniec, M.; Tao, F. F.; Room-temperature catalytic oxidation of formaldehyde on catalysts. *Catal. Sci. Technol*. **2016**, 6, 3649–3669.
3. Guo, J. H.; Lin, C. X.; Jiang, C. J.; Zhang, P. Y.; Review on noble metal-based catalysts for formaldehyde oxidation at room temperature. Appl. Surf. Sci. **2019**, 475, 237–255.
4. Zhu, S.; Wang, J.; Nie, L.; Progress of Catalytic Oxidation of Formaldehyde over Manganese Oxides. *Chemistry Select* **2019**, 4, 12085–12098.
5. Miao, L.; Wang, J.; Zhang, P.; Review on manganese dioxide for catalytic oxidation of airborne formaldehyde. *Appl. Surf. Sci*. **2019**, 466, 441–453.
6. An, G.F.; Huang, Q.; Li, X.; Mao, J.J.; Wei, C.; Yang, B.; Li, D.W.; Chen, M.D.; Tao, T.; and Yang, H.; Efficiently enhancing stability for a low concentration HCHO degradation using hexagonal prism MnCe-MOFs catalysts. *Materials Chemistry and Physics*, **2024**, 328, 130027.
7. Liang, W.; Long-term indoor formaldehyde variations and health risk assessment in Chinese urban residences following renovation. *Building and environment*, **2021**, 206, 108402.
8. Song, J.; Ren, X.; Hu, G.; Wang, L.; Hu, X.; Enhanced photocatalytic degradation of indoor formaldehyde by sepiolite decorated with TiO_2 nanoparticles: Effects of key preparation parameters. *Microporous and Mesoporous Materials*, **2023**, *353*, 112515.
9. Zhu, Z.; Wu, R.J.; The degradation of formaldehyde using a Pt@TiO2 nanoparticles in presence of visible light irradiation at room temperature. *Journal of the Taiwan Institute of Chemical Engineers*, **2015**, *50*, 276-281.

 doi:10.20944/preprints202605.1224.v1

10. Guo, Y.; Gao, P.; Han, Q.; Feng, L.; and Zhang, L.; Enhancing visible light degradation of gaseous formaldehyde with CuOx/OVs-TiO2 photocatalyst loaded wallpaper: Preparation, efficacy and mechanism. *Chemosphere*, **2025**, 371, 144051.
11. Zeng, X.; Zeng, Z.; Hu, Q.; Liu, K.; Ming, L.; Cheng, B.; Wang, W.; Luo, G.; and Cao, S.; Hierarchical Pt/NiO hollow nanofibers for catalytic oxidation of HCHO at room temperature. *Chinese Journal of Structural Chemistry*, **2025**, 100575.
12. Bai, H.; Synthesis of Bi_2S_3-TiO_2 nanocomposite and its electrochemical and enhanced photocatalytic properties for phenol degradation. International *Journal of Electrochemical Science*, **2023**, 100071.
13. Wang, Y.; Zhang, Y.; Liu, Y.; Wu, Z.; Fluorine-induced oxygen vacancies on TiO_2 nanosheets for photocatalytic indoor VOCs degradation. *Applied Catalysis B: Environmental*, **2022**, 316, 121610.
14. Mu, Y.-L.; He, Q.; Li, C.-Y.; Sheng, D.; Wu, S.-H.; Liu, Y.; Ren, H.-T.; Han, X. Contributions of Surface Oxidizing Species and Cu^+ to the Antibacterial Activities of Cu_2O with Different Crystalline Structures. *Langmuir* **2024**, 40, 17909–17918.
15. Li, Y.; Wang, B.; Liu, S.; Duan, X.; Hu, Z. Synthesis and Characterization of Cu_2O/TiO_2 Photocatalysts for H_2 Evolution from Aqueous Solution with Different Scavengers. *Appl. Surf. Sci.* **2015**, 324, 736–744.
16. Acharya, R.; Pati, S.; Parida, K.; A review on visible light driven spinel ferrite-g-C3N4 photocatalytic systems with enhanced solar light utilization. *Journal of Molecular Liquids*, **2022**, 357, 119105.
17. Acharya, R.; Acharya, L.; Parida, K.; BiFeO 3 -Based Materials For Augmented Photoactivity, *Perovskite Materials for Energy and Environmental Applications*. **2022**, 167-216.
18. Mansingh, S.; Sultana, S.; Acharya, R.; Ghosh, M.K.; Parida, K.M.; Efficient Photon Conversion via Double Charge Dynamics CeO2–BiFeO3 p–n Heterojunction Photocatalyst Promising toward N2 Fixation and Phenol–Cr(VI) Detoxification. *Inorganic Chemistry*, **2020**, 59, 3856-3873.
19. Xie, S.; Wang, Z.; Cheng, F.; Zhang, P.; Mai, W.; Tong, Y.; Ceria and ceria-based nanostructured materials for photoenergy applications. *Nano Energy*, **2017**, 34, 313-337.
20. Arul, N.S.; Mangalaraj, D.; Ramachandran, R.; Grace, A.N.; Han, J.I.; Fabrication of CeO2/Fe2O3 composite nanospindles for enhanced visible light driven photocatalysts and supercapacitor electrodes. *Journal of Materials Chemistry A*, **2015**, 3, 15248-15258.
21. Sreeremya, T.S.; Krishnan, A.; Remani, K.C.; Patil, K.R.; Brougham, D.F.; Ghosh, S.; Shape-Selective Oriented Cerium Oxide Nanocrystals Permit Assessment of the Effect of the Exposed Facets on Catalytic Activity and Oxygen Storage Capacity. *ACS Applied Materials & Interfaces*, **2015**, 7, 8545-8555.
22. Paier, J.; Penschke, C.l; and Sauer, J.; Oxygen Defects and Surface Chemistry of Ceria: Quantum Chemical Studies Compared to Experiment. *Chemical Reviews*, **2013**, 113, 3949-3985.
23. Wetchakun, N.; Chaiwichain, S.; Inceesungvorn, B.; Pingmuang, K.; Phanichphant, S.; Minett, A.I.; and Chen, J.; BiVO4/CeO2 Nanocomposites with High Visible-Light-Induced Photocatalytic Activity. *ACS Applied Materials & Interfaces*, **2012**, 4, 3718-3723.
24. Chaiwichian, S.; Inceesungvorn, B.; Pingmuang, K.; Wetchakun, K.; Phanichphant, S.; and Wetchakun, N.; Synthesis and Characterization of the Novel BiVO4/CeO2 Nanocomposites. *Engineering Journal*, **2012**, 16, 153-160
25. Li, K.; Ji, J.; He, M.; and Huang, H.; Complete oxidation of formaldehyde over a Pd/CeO2 catalyst at room temperature: tunable active oxygen species content by non-thermal plasma activation. *Catalysis Science & Technology*, **2020**, 10, 6257-6265.
26. Zhu, Z.; Lin, Y.C.; Chung, C.L.; Wu, R.J.; and Huang, C.L.; A novel composite of triangular silver nanoplates on BiVO4 for gaseous formaldehyde degradation. *Applied Surface Science*, **2021**, 543, 148784.
27. Zhang, G.; Sun, Z.; Duan, Y.; Ma, R.; Zheng, S.; Synthesis of nano-TiO2/diatomite composite and its photocatalytic degradation of gaseous formaldehyde. *Applied Surface Science*, **2017**, 412, 105-112.
28. Hu, X.; Li, C.; Sun, Z.; Song, J.; Zheng, S.; Enhanced photocatalytic removal of indoor formaldehyde by ternary heterogeneous BiOCl/TiO2/sepiolite composite under solar and visible light. *Building and Environment*, **2020**, 168, 106481.
29. Lu, C.C.; Alshahrani, T.; Wu, R.J.; Fegade, U.; Jethave, G.; Al-Ahmed, A.; Khan, F.; Kolate, S.; Synthesis of CeO2–BiVO4 nano photocatalyst material and used for the degradation of gaseous formaldehyde. *Optical Materials*, **2023**, 144, 114310.

 doi:10.20944/preprints202605.1224.v1

30. Wu, P.; Attarde, S.; Lu, C.C.; Wu, R.J.; Fegade, U.; Kolate, S.; Patil, N.; Altalhi, T.; ZnMn2O4-BiVO4 as Photocatalyst for Degradation of Gaseous HCHO Using Daylight. *ChemistrySelect*, **2024**, *9*, e202401501.
31. Zhang, G.; Sun, Z.; Duan, Y.; Ma, R.; and Zheng, S.; Synthesis of nano-TiO2/diatomite composite and its photocatalytic degradation of gaseous formaldehyde. Applied Surface Science, 2017, 412, 105-112.
32. Suhong, L.U.; Fan, W.A.N.G.; Canchang, C.H.E.N.; and Kelun, L.I.; Catalytic oxidation of formaldehyde over CeO2-Co3O4 catalysts. Journal of Rare Earths, 2017, 35, 867-874.
33. Liang, W.; Long-term indoor formaldehyde variations and health risk assessment in Chinese urban residences following renovation. Building and Environment, 2021, 206, 108402.